Supplementary Information

The shift current photovoltaic effect response in Wurtzite and Zincblende semiconductors via first-principles calculation

Yu Qiu[1], Yong Sun[1], Hui-Xue Shen[1], Huixia Fu[2]*, Man-Yi Duan[1], Cai Cheng[1,3,]*

[1] School of Physics and Electronic Engineering, Sichuan Normal University, Chengdu 610101, China

[2]Center of Quantum Materials and Devices, College of Physics, Chongqing University, Chongqing 401331, China

[3] School of Materials and Energy, State Key Laboratory of Electronic Thin Film and Integrated Devices, University of Electronic Science and Technology of China, Chengdu 610054, China

*Address correspondence to hxfu@cqu.edu.cn; ccheng@sicnu.edu.cn

Table S1. Lattice constants of seven materials with wurtzite structure

	AgI	CdSe	CdTe	**GaAs**	ZnSe	ZnTe	SiGe
Our work							
a=*b*	4.69	4.399	4.68	**4.05**	4.05	4.36	3.94
c	7.66	7.169	7.67	**6.67**	6.65	7.18	6.50
Other calc							
a=*b*	4.69[1]	4.279[2]	4.60	**4.05**[3]	3.98[4]	4.27[5]	
c	7.64	6.98	7.53	**6.67**	6.53	6.99	
Experiment							
a=*b*	4.60[6]	4.32[7]			3.99[8]		
c	7.52	7.20			6.55		

Table S2. Lattice constants of seven materials with zincblende structure

	AgI	CdSe	CdTe	**GaAs**	ZnSe	ZnTe	SiGe
Our work	6.62	6.20	6.63	**5.75**	5.74	6.18	5.60
Other calc.	6.61[1]	6.04[9]	6.61[10]	**5.75**[3]	5.74[11]	6.18[12]	5.60[13]
Experiment	6.50[6]	6.13[7]	6.48	**5.65**[14]	5.67	6.10[11]	

Table S3. The calculated Bader Charge (unit: e^-)

	AgI		CdSe		CdTe		GaAs		ZnSe		ZnTe		SiGe	
	Ag	I	Cd	Se	Cd	Te	Ga	As	Zn	Se	Zn	Te	Si	Ge
Wur-	-0.28	+0.28	-0.7	+0.7	-0.52	+0.52	-0.66	+0.66	-0.71	+0.71	-0.52	+0.52	-0.24	+0.24
Zin-	-0.25	+0.25	-0.7	+0.7	-0.5	+0.5	-0.62	+0.62	-0.74	+0.7	-0.5	+0.5	-0.25	+0.25

Table S4. The bond length for the wurtzite and zincblende structures (unit: Å)

	Ag-I	Cd-Se	Cd-Te	Ga-As	Zn-Se	Zn-Te	Si-Ge
Wur-(z-axis)	2.87	2.69	2.87	2.49	2.49	2.68	2.43
Zin-[111]	2.87	2.69	2.87	2.49	2.49	2.69	2.42

Table S5. POSCAR file of wurtzite and zincblende structure GaAs, where Zincblende structure contains primitive cells and unit cells.

GaAs Wurtzite Primitive Cell

```
1.0
        4.0528001785        0.0000000000        0.0000000000
       -2.0264000893        3.5098279111        0.0000000000
        0.0000000000        0.0000000000        6.6708002090
   Ga    As
    2     2
Direct
      0.333333343         0.666666687         0.999830008
      0.666666627         0.333333313         0.499830008
      0.333333343         0.666666687         0.374170005
      0.666666627         0.333333313         0.874170005
```

GaAs Zincblende Primitive Cell

```
   1.0
    -0.0000000000000000     2.8752572761656805     2.8752572761656805
     2.8752572761656805    -0.0000000000000000     2.8752572761656805
     2.8752572761656805     2.8752572761656805     0.0000000000000000
   Ga    As
   1     1
Direct
  0.0000000000000000  0.0000000000000000  0.0000000000000000
  0.2500000000000000  0.2500000000000000  0.2500000000000000
```

GaAs Zincblende Unit Cell

```
   1.0
     5.7511750878594086     0.0000000000000000     0.0000000000000000
     0.0000000000000000     5.7511750878594086     0.0000000000000000
     0.0000000000000000     0.0000000000000000     5.7511750878594086
   Ga    As
   4     4
Direct
  0.0000000000000000  0.0000000000000000  0.0000000000000000
  0.0000000000000000  0.5000000000000000  0.5000000000000000
  0.5000000000000000  0.0000000000000000  0.5000000000000000
  0.5000000000000000  0.5000000000000000  0.0000000000000000
  0.2500000000000000  0.2500000000000000  0.7500000000000000
  0.2500000000000000  0.7500000000000000  0.2500000000000000
  0.7500000000000000  0.2500000000000000  0.2500000000000000
  0.7500000000000000  0.7500000000000000  0.7500000000000000
```

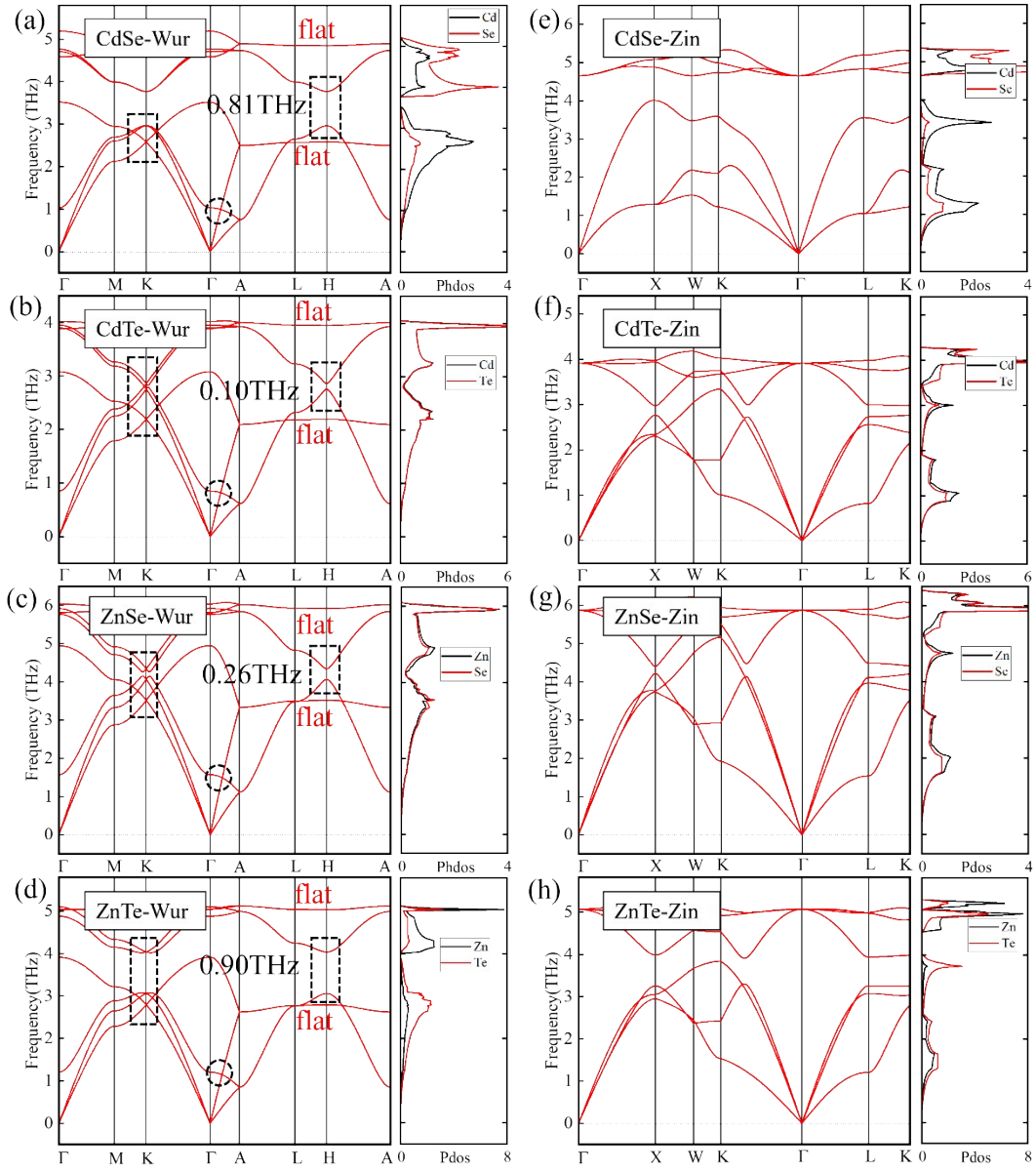

Fig S1. Phonon spectrum and phonon density of states (PhDOS). (a)-(d) The phonon spectrum and the corresponding PhDOS of CdSe CdTe ZnSe ZnTe with wurtzite structures, respectively. (e)-(h) The phonon spectrum and the corresponding PhDOS of CdSe CdTe ZnSe ZnTe with zincblende structures, respectively.

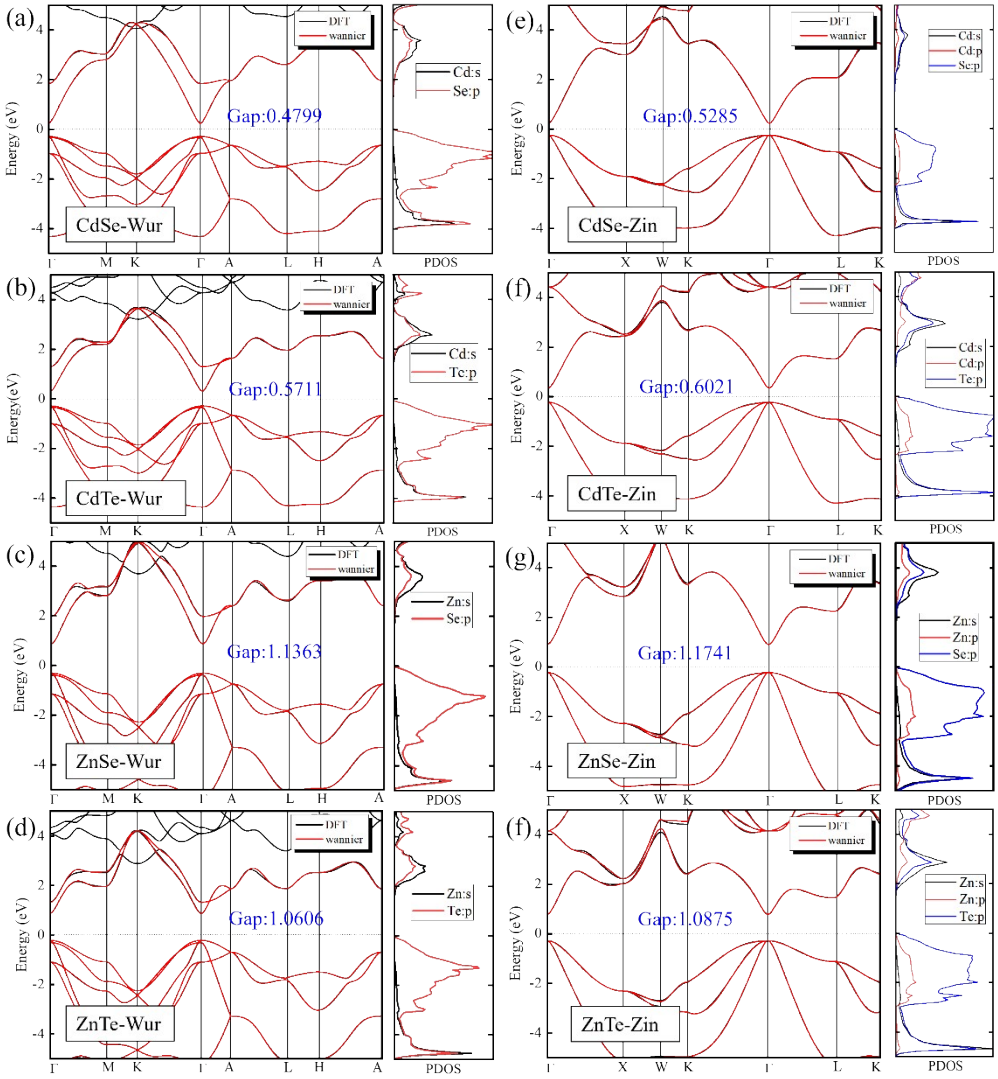

Fig S2. Band structures and the corresponding partial density of states (PDOS). (a-d) The band structures and the corresponding partial density of states (PDOS) of CdSe CdTe ZnSe ZnTe wurtzite, respectively. (e-h) The band structures and corresponding partial density of states (PDOS) of CdSe CdTe ZnSe ZnTe zincblende, respectively. All band structures contain the calculation results of DFT (indicated by the black line) and the results of Wannier interpolation fitting (indicated by the red line).

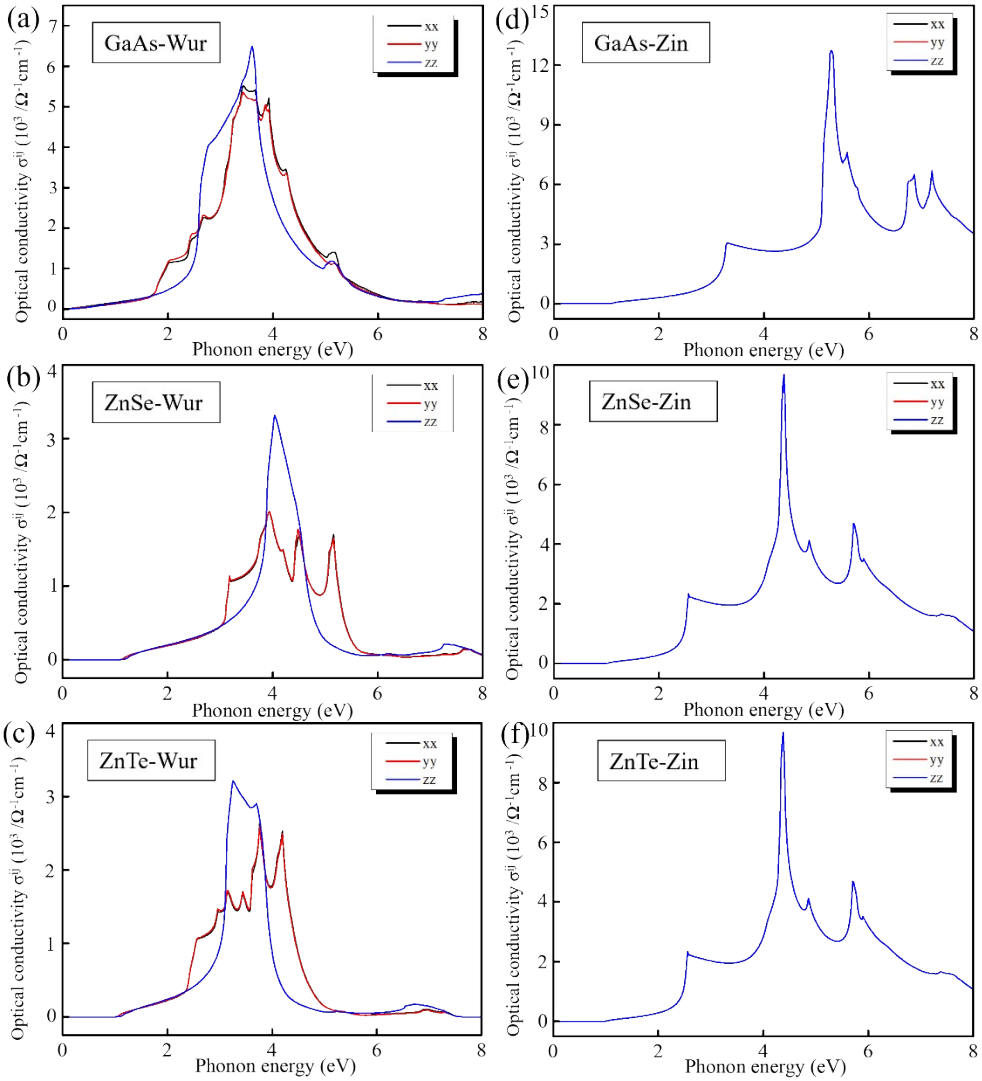

Fig S3. All non-zero linear optical conductivity tensor components in GaAs, ZnSe, and ZnTe. (a-c) The linear optical conductivity of wurtzite structure GaAs, ZnSe, and ZnTe in three different directions. (d-f) The linear optical conductivity of zincblende structure GaAs, ZnSe, and ZnTe in three different directions.

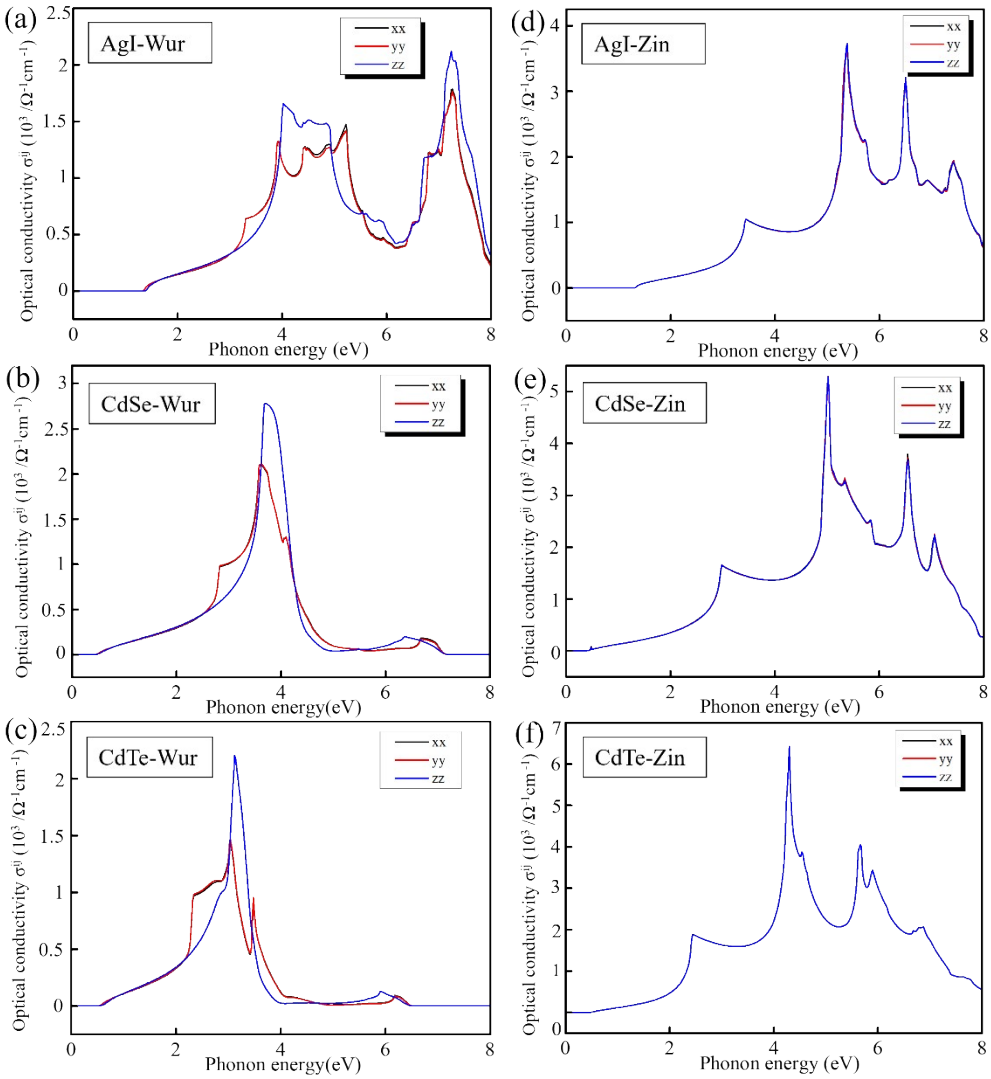

Fig S4. All non-zero linear optical conductivity tensor components in AgI, CdSe, and CdTe. (a-c) The linear optical conductivity of wurtzite structure AgI, CdSe, and CdTe in three different directions. (d-f) The linear optical conductivity of zincblende structure AgI, CdSe, and CdTe in three different directions,

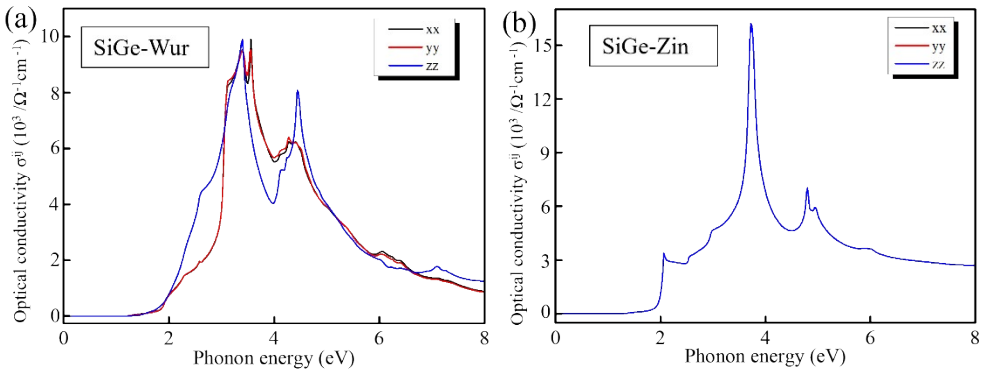

Fig S5. All non-zero linear optical conductivity tensor components in the SiGe. (a) (b) The linear optical conductivity of different directional components of SiGe with wurtzite and zincblende structure respectively.

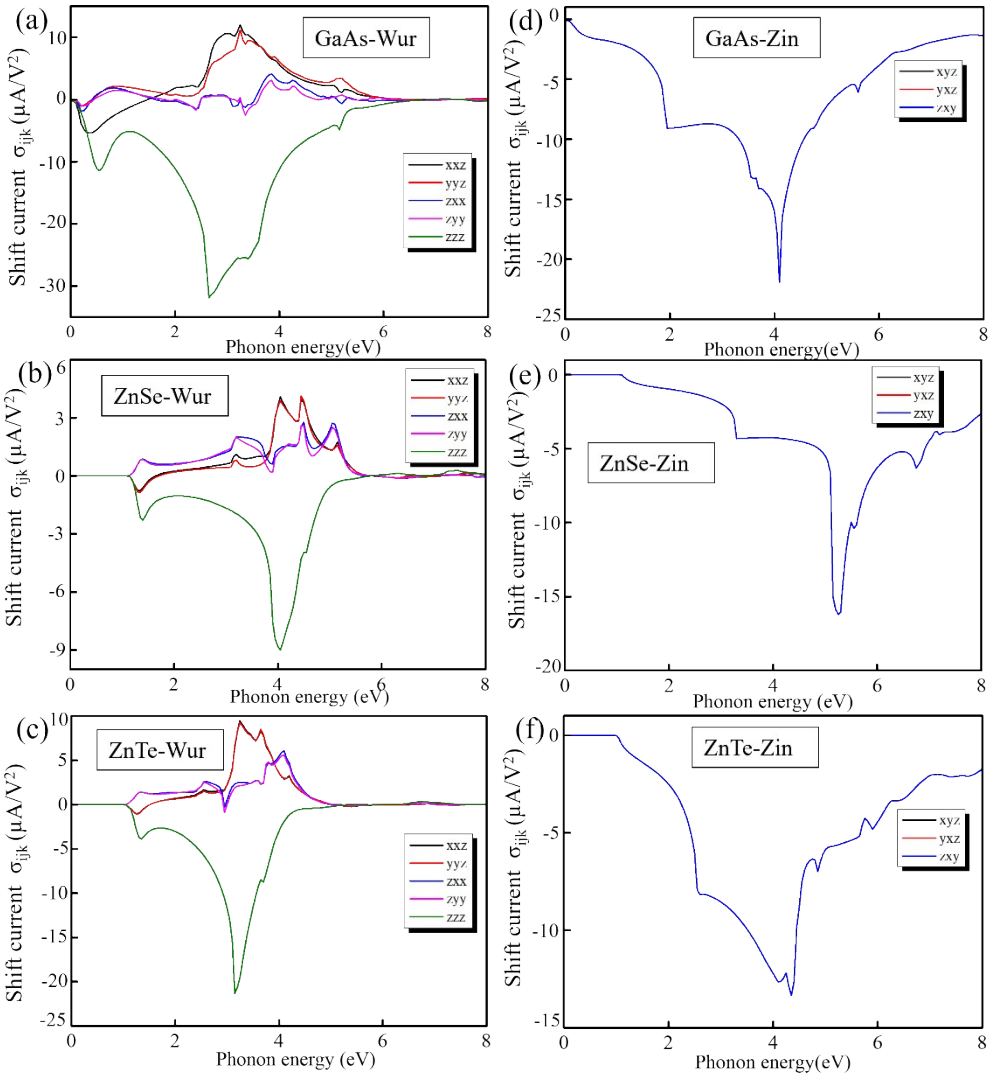

Fig S6. All non-zero shift current tensor components in the GaAs, ZnSe, and ZnTe. (a)-(b) The shift current components of GaAs, ZnSe, and ZnTe wurtzite structures that are not zero. (e)-(h) The shift current components of GaAs, ZnSe, and ZnTe zincblende structures that are not zero, respectively. Different colors represent components in different directions, and *ijk* represents *xyz*.

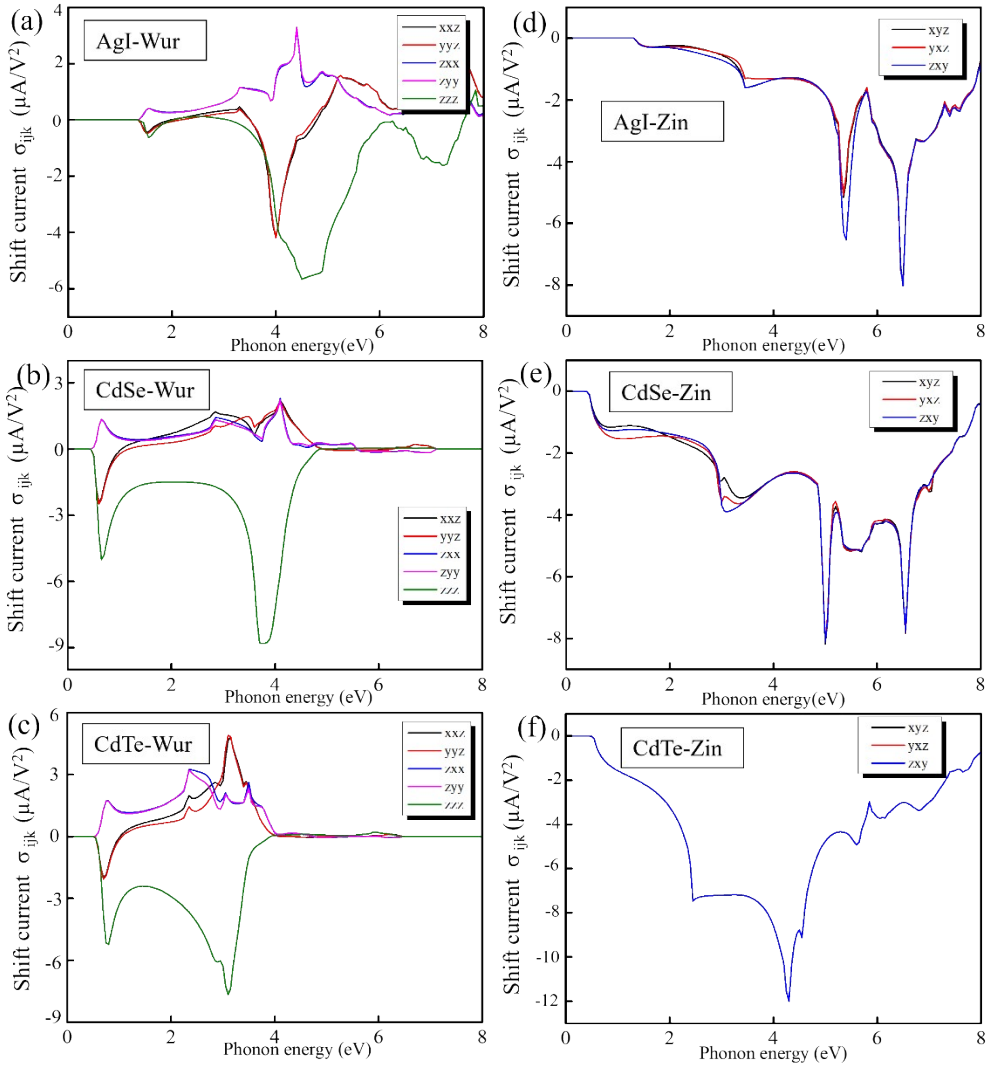

Fig S7. All non-zero shift current tensor components in the AgI, CdSe, and CdTe. (a)-(b) The shift current tensor components of AgI, CdSe, and CdTe wurtzite structures that are not zero. (e)-(h) The shift current tensor components of AgI, CdSe, and CdTe zincblende structures that are not zero, respectively. Different colors represent components in different directions, and *ijk* represents *xyz*.

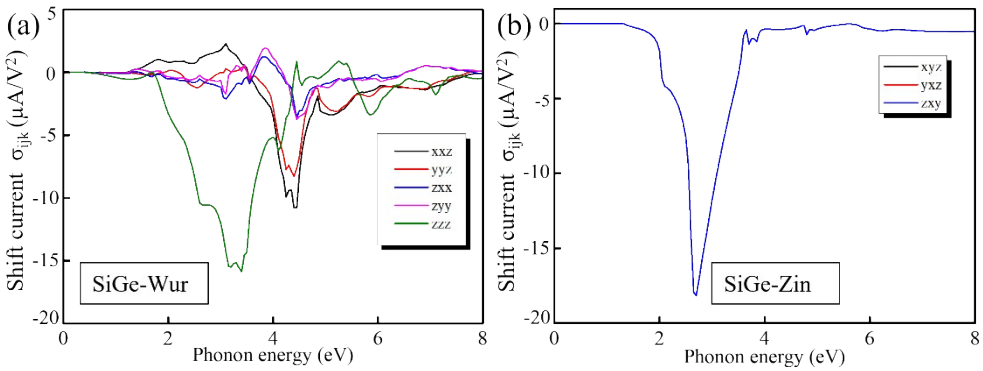

Fig S8. All non-zero shift current tensor components in the SiGe. (a) (b) Represent the shift current tensor components of the SiGe with wurtzite and zincblende structure respectively, and the *ijk* represents *xyz*.

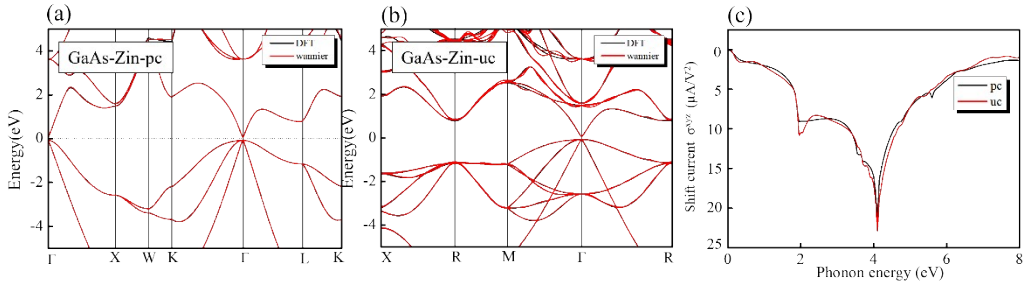

Fig S9. The shift current response between the primitive and unit cell. (a) (b) The band structures of the primitive cell and unit cell of the zincblende structure (including DFT result and wannier interpolation fitting). (c) The maximum shift current *zzz* component comparison between unit cell and primitive cell. The Wannier90 interpolation selects the *s* and *p* orbitals of Ga, as well as the *p* orbitals of As.

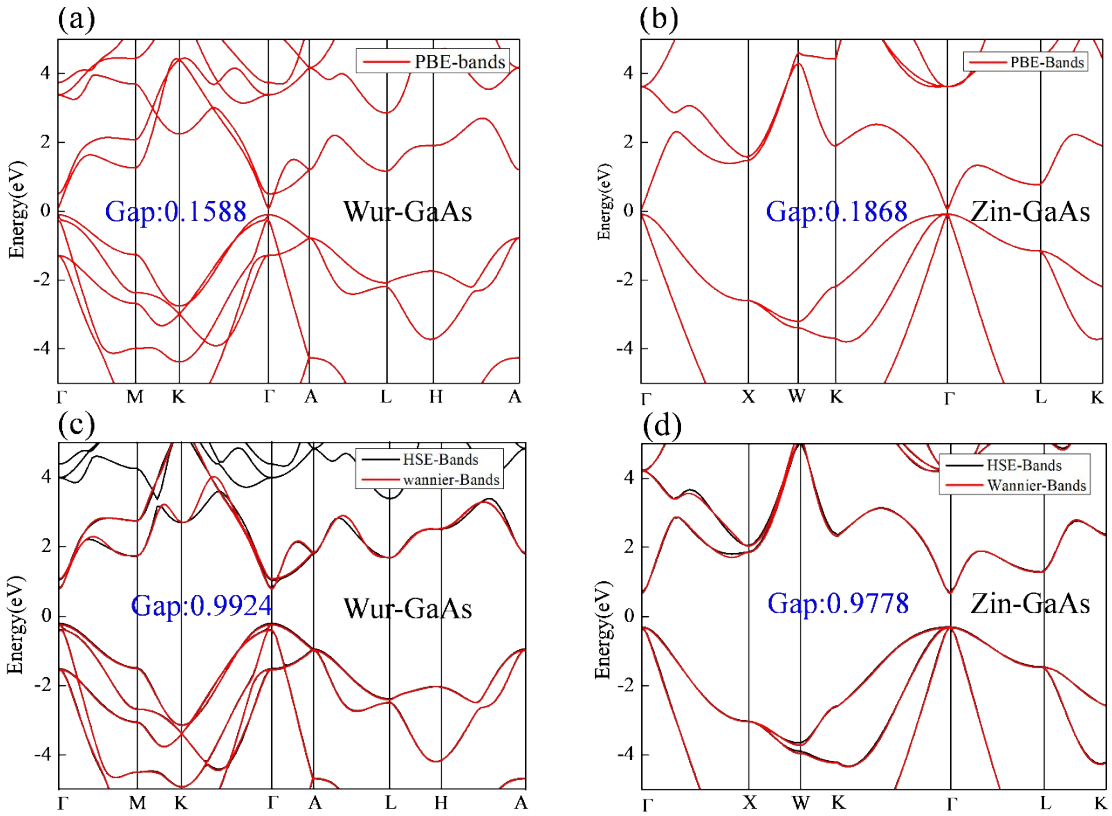

Fig S10. Band structure between the PBE and the HSE functional level. (a-b) The band structures of wurtzite and zincblende structure. (c-d) The Wannier90 interpolation selects the *s* and *p* orbitals of Ga, as well as the *p* orbitals of As, under the HSE functional level.

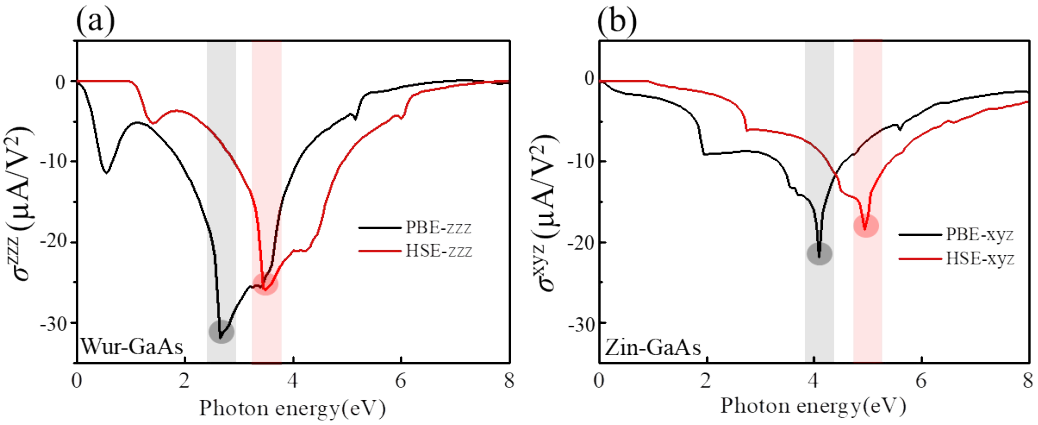

Fig S11. Shift current spectrum of bulk GaAs in wurizite and zincblende structures. (a) wurtzite (space group 186) structure with the maximum shift current *zzz* component. (b) zincblende (space group 216) structures with the maximum shift current *xyz* component.

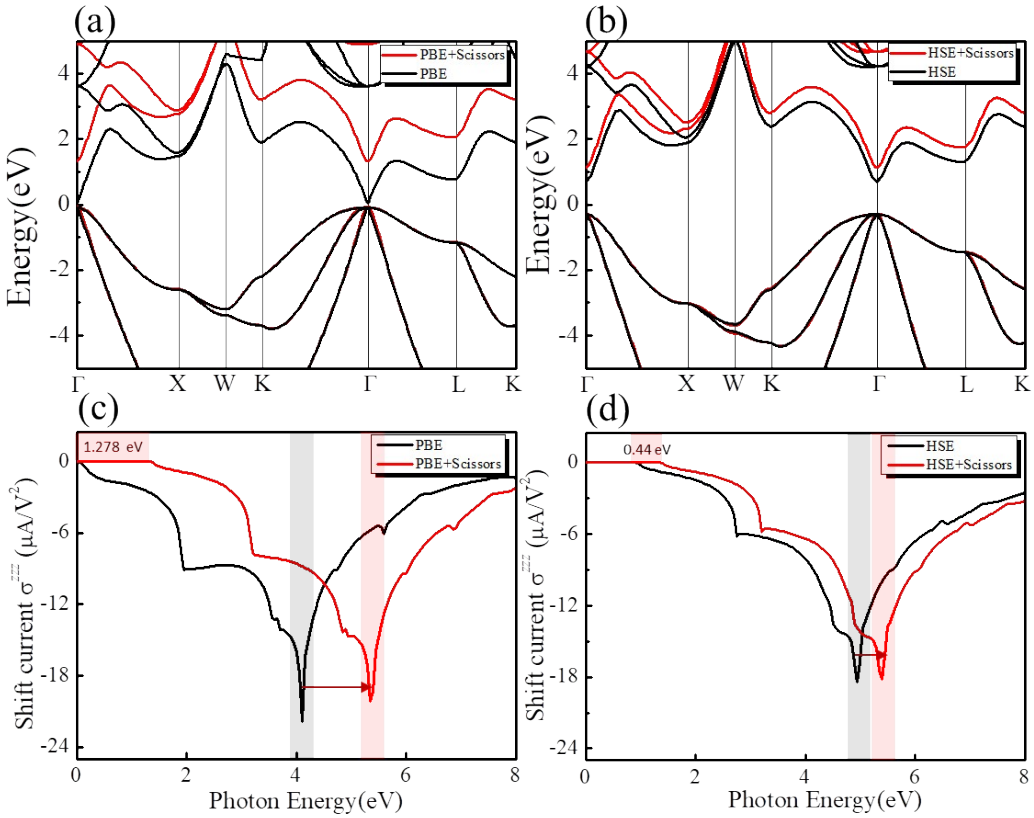

Fig. S12. Band structure and shift current of the Zincblende bulk GaAs under the scissors operator. (a-b) Band structure at the PBE and HSE levels. (c-d) Shift current in the zzz direction at the PBE and HSE level. The PBE scissors operation results in a band gap of 1.278 eV, while the HSE value is 0.44 eV.

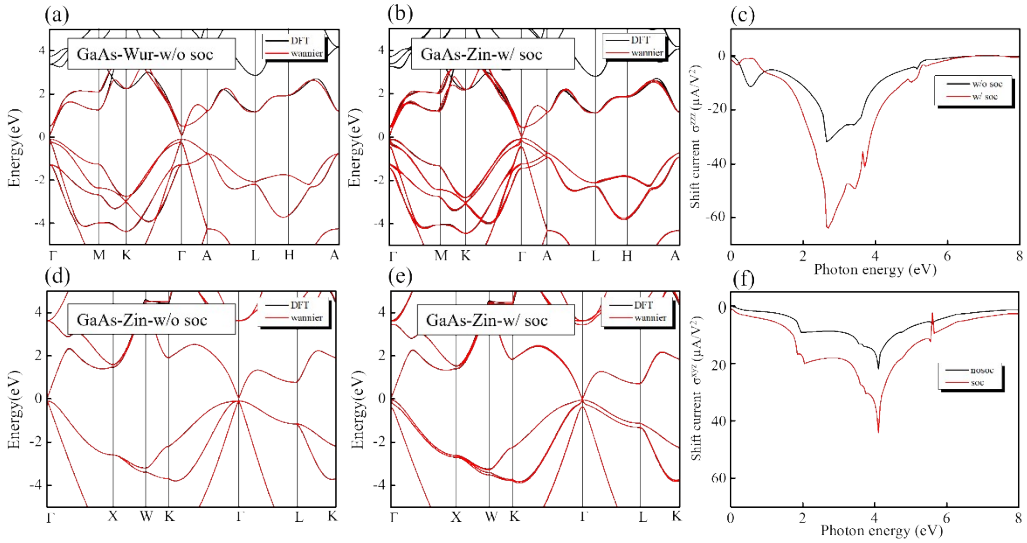

Fig S13. The shift current response to whether the SOC effect is considered. (a-b) The band structures without and with SOC of the wurtzite structure of GaAs. (c) The maximum shift current *zzz* component without and with SOC is considered. (d-e) The band structures without and with SOC of the zincblende structure of GaAs. (f) The maximum shift current *xyz* component without and with SOC is considered. Both the band structures contain the DFT and Wannier90 interpolation results. The GaAs of wurtzite select the s orbital of Ga and the *p* orbital of As, and the GaAs of zincblende select the *s* orbital and *p* orbital of Ga and the *p* orbital of As.

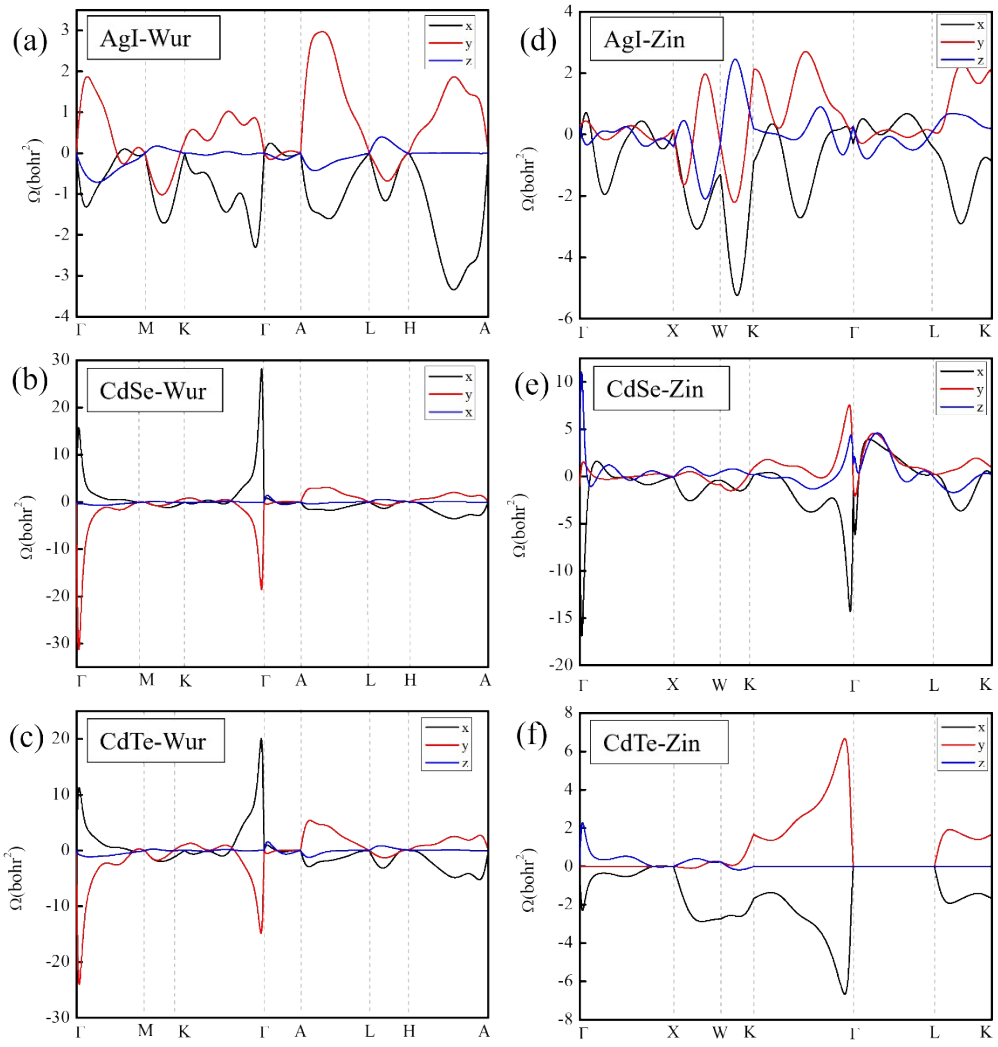

Fig S14. The berry curvature of AgI, CdSe, and CdTe along the high symmetry point path. (a-c) The berry curvature of AgI, CdSe, and CdTe with the wurtzite structure. (d-f) The berry curvature of AgI, CdSe, and CdTe with the zincblende structure. The black, red, and blue segments represent the berry curvature in the *x*, *y*, and *z* directions, respectively.

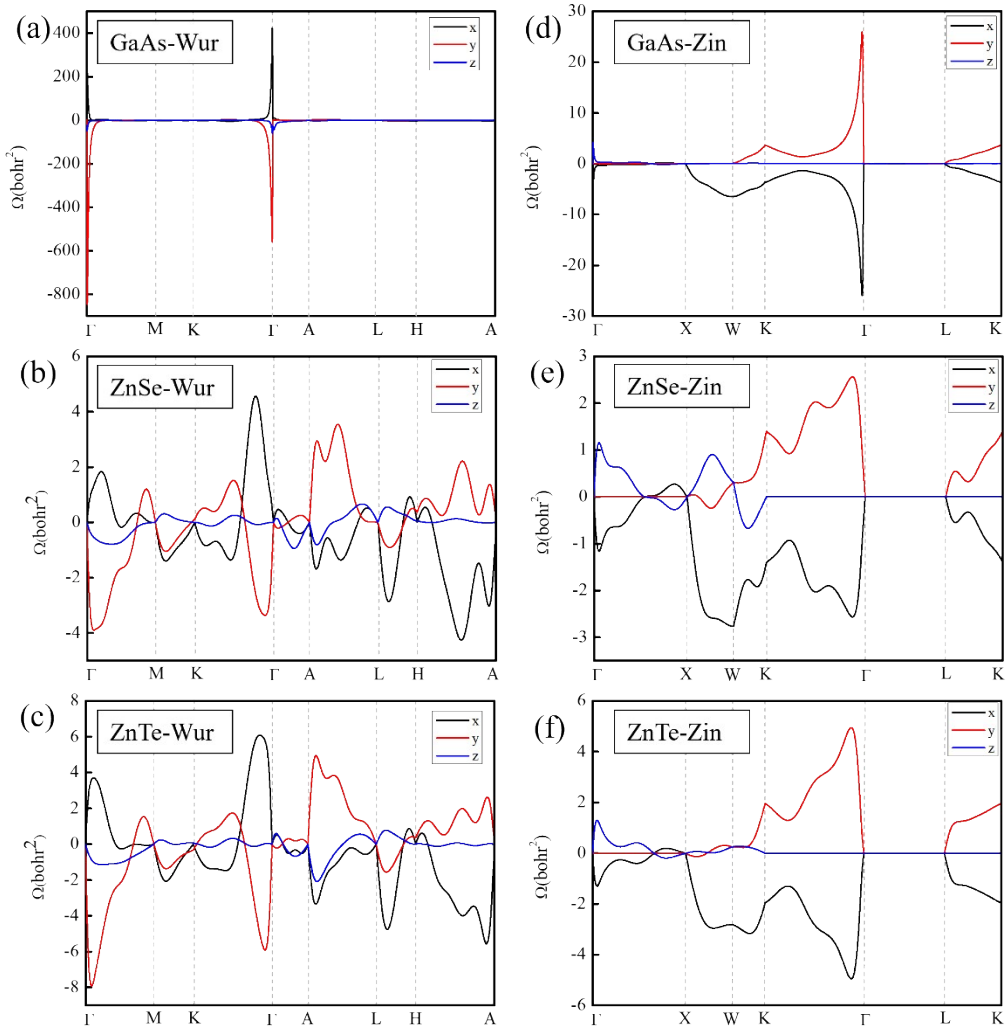

Fig S15. The berry curvature of GaAs, ZnSe, and ZnTe along the high symmetry point path. (a-c) The berry curvature of AgI, ZnSe, and ZnTe with the wurtzite structure. (d-f) The berry curvature of GaAs, ZnSe, and ZnTe with the zincblende structure. The black, red, and blue segments represent the berry curvature in the *x*, *y*, and *z* directions, respectively.

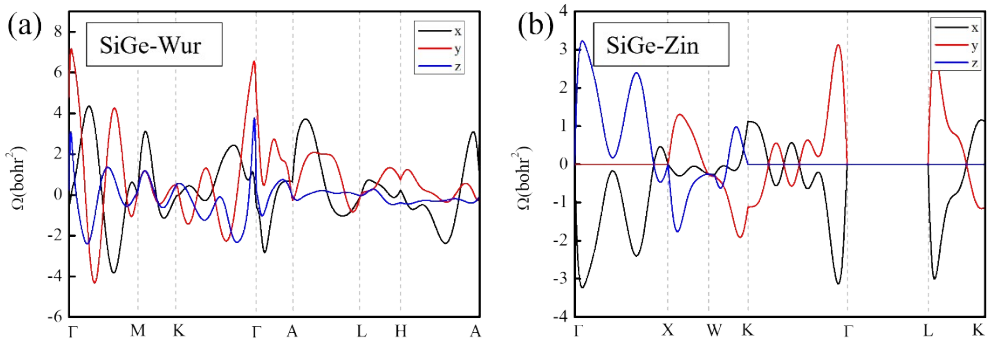

Fig S16. The berry curvature of SiGe along the high symmetry point path. The black, red, and blue segments represent the berry curvature in the *x*, *y*, and *z* directions, respectively.

Symmetry analysis

We use these two formulas to determine all the non-zero components of the linear photoconductivity tensor and the shift current tensor[15].

$$\Lambda_{ij} = |R| R_{ii'} R_{jj'} \Lambda_{i'j'}$$
$$\Gamma_{ijk} = R_{ii'} R_{jj'} R_{kk'} \Gamma_{i'j'k'}$$

Wurtzite structure: Linear optical conductivity tensor

The wurtzite is the space group 186, with a point group of C_{6v}, and its tensor is greatly influenced by the following three symmetric operations. Includes two mirror symmetry M_x M_y and one rotational symmetry operation C_{6v}.

$$M_y = \begin{pmatrix} -1 & 0 & 0 \\ 0 & 1 & 0 \\ 0 & 0 & 1 \end{pmatrix} \quad M_x = \begin{pmatrix} 1 & 0 & 0 \\ 0 & -1 & 0 \\ 0 & 0 & 1 \end{pmatrix} C_{6z} = \frac{1}{2}\begin{pmatrix} 1 & \sqrt{3} & 0 \\ -\sqrt{3} & 1 & 0 \\ 0 & 0 & 2 \end{pmatrix}$$

The linear optical conductivity is a second-order tensor

$$\sigma_{ij} = \begin{pmatrix} \sigma_{xx} & \sigma_{xy} & \sigma_{xz} \\ \sigma_{yx} & \sigma_{yy} & \sigma_{yz} \\ \sigma_{zx} & \sigma_{zy} & \sigma_{zz} \end{pmatrix}$$

The M_y leads that linear optical conductivity tensor is

$$\sigma_{ij} = \begin{pmatrix} \sigma_{xx} & 0 & 0 \\ 0 & \sigma_{yy} & \sigma_{yz} \\ 0 & \sigma_{zy} & \sigma_{zz} \end{pmatrix}$$

Then, the M_y leads that linear optical conductivity tensor is

$$\sigma_{ij} = \begin{pmatrix} \sigma_{xx} & 0 & 0 \\ 0 & \sigma_{yy} & 0 \\ 0 & 0 & \sigma_{zz} \end{pmatrix}$$

Last, the C_{6z} leads that linear optical conductivity tensor should be

$$\sigma_{ij} = \begin{pmatrix} \sigma_{xx} & 0 & 0 \\ 0 & \sigma_{yy} & 0 \\ 0 & 0 & \sigma_{zz} \end{pmatrix}$$

and $\sigma_{xx} = \sigma_{yy}$

Wurtzite structure: Shift current tensor

The shift current, initially a three-order tensor containing a total of 27 elements, is subsequently reduced by eliminating symmetric quantities within the matrix, resulting in a further reduction to 18 components.

$$\sigma_{ijk}=\begin{pmatrix}\sigma_{xxx} & \sigma_{xxy} & \sigma_{xxz} & \sigma_{xyy} & \sigma_{xyz} & \sigma_{xzz}\\ \sigma_{yxx} & \sigma_{yxy} & \sigma_{yxz} & \sigma_{yyy} & \sigma_{yyz} & \sigma_{yzz}\\ \sigma_{zxx} & \sigma_{zxy} & \sigma_{zxz} & \sigma_{zyy} & \sigma_{zyz} & \sigma_{zzz}\end{pmatrix}$$

The space group of Wurtzite is No.186 and the point group is C_{6v}. Wurtzite belongs to space group 216 and has a point group of C_{6v}. Within this crystal structure, three primary symmetry operations play a pivotal role in determining the characteristics of the shift current tensor.

$$M_{zy}=\begin{pmatrix}-1 & 0 & 0\\ 0 & 1 & 0\\ 0 & 0 & 1\end{pmatrix}\quad M_{zx}=\begin{pmatrix}1 & 0 & 0\\ 0 & -1 & 0\\ 0 & 0 & 1\end{pmatrix}\quad C_{6z}=\frac{1}{2}\begin{pmatrix}1 & \sqrt{3} & 0\\ -\sqrt{3} & 1 & 0\\ 0 & 0 & 2\end{pmatrix}$$

The above three symmetries cause the shift current tensor to be

$$\sigma_{ijk}=\begin{pmatrix}0 & 0 & \sigma_{xxz} & 0 & 0 & 0\\ 0 & 0 & 0 & 0 & \sigma_{yyz} & 0\\ \sigma_{zxx} & 0 & 0 & \sigma_{zyy} & 0 & \sigma_{zzz}\end{pmatrix}$$

Due to the symmetry of C_{6v}

$$\sigma_{xxz}=R_{xx}R_{xx}R_{zz}\sigma_{xxz}+R_{xx}R_{xy}R_{zz}\sigma_{xyz}+R_{xy}R_{xx}R_{zz}\sigma_{yxz}+R_{xy}R_{xy}R_{zz}\sigma_{yyz}$$
$$=\frac{1}{8}\left[(1)(1)(2)\sigma_{xxz}+(3)(2)\sigma_{yyz}\right]$$
$$=\frac{1}{4}\left[\sigma_{xxz}+3\sigma_{yyz}\right]$$

$$\sigma_{yyz}=R_{yy}R_{yy}R_{zz}\sigma_{yyz}+R_{yy}R_{yx}R_{zz}\sigma_{yxz}+R_{yx}R_{yy}R_{zz}\sigma_{xyz}+R_{yx}R_{yx}R_{zz}\sigma_{xxz}$$
$$=\frac{1}{8}\left[(1)(1)(2)\sigma_{yyz}+(3)(2)\sigma_{xxz}\right]$$
$$=\frac{1}{4}\left[\sigma_{yyz}+3\sigma_{xxz}\right]$$

$$\sigma_{zxx} = R_{zz}R_{xx}R_{xx}\sigma_{zxx} + R_{zz}R_{xx}R_{xy}\sigma_{zxy} + R_{zz}R_{xy}R_{xx}\sigma_{zyx} + R_{zz}R_{xy}R_{xy}\sigma_{zyy}$$

$$= \frac{1}{8}\left[(2)(1)(1)\sigma_{zxx} + (2)\left(\sqrt{3}\right)\left(\sqrt{3}\right)\sigma_{zyy} \right]$$

$$= \frac{1}{4}\left[\sigma_{zxx} + 3\sigma_{zyy} \right]$$

$$\sigma_{zyy} = R_{zz}R_{yy}R_{yy}\sigma_{zyy} + R_{zz}R_{yy}R_{yx}\sigma_{zyx} + R_{zz}R_{yx}R_{yy}\sigma_{zxy} + R_{zz}R_{yx}R_{yx}\sigma_{zxx}$$

$$= \frac{1}{8}\left[(2)(1)(1)\sigma_{zyy} + (2)\left(-\sqrt{3}\right)\left(-\sqrt{3}\right)\sigma_{zxx} \right]$$

$$= \frac{1}{4}\left[\sigma_{zzyy} + 3\sigma_{zxx} \right]$$

$$\sigma_{zzz} = R_{zz}R_{zz}R_{zz}\sigma_{zzz} = \sigma_{zzz}$$

$$\sigma_{xxz} = \sigma_{yyz}$$

$$\sigma_{zxx} = \sigma_{zyy}$$

Hence, in the Wurtzite structure, there exist five linear photoconductivity components $\sigma_{xxz}, \sigma_{yyz}, \sigma_{zxx}, \sigma_{yyz}$ and σ_{zzz} (including two pairs of equal components $\sigma_{xxz} = \sigma_{yyz}, \sigma_{zxx} = \sigma_{zyy}$) that are non-zero.

Zincblende structure: Linear optical conductivity tensor

Zincblende belongs to space group No.216 with a T_d point group. Within this context, the linear photoconductivity is represented by a first-order tensor. Crucially, six symmetry operations play a pivotal role in influencing both the linear photoconductivity tensor and the shift current tensor. These operations consist of three rotational symmetries and three mirror symmetries.

$$C_{2z}=\begin{pmatrix}-1 & 0 & 0\\ 0 & -1 & 0\\ 0 & 0 & 1\end{pmatrix}\quad C_{2x}=\begin{pmatrix}1 & 0 & 0\\ 0 & -1 & 0\\ 0 & 0 & -1\end{pmatrix}\quad C_{2y}=\begin{pmatrix}-1 & 0 & 0\\ 0 & 1 & 0\\ 0 & 0 & -1\end{pmatrix}$$

$$M_{xy}=\begin{pmatrix}0 & 1 & 0\\ 1 & 0 & 0\\ 0 & 0 & 1\end{pmatrix}\quad M_{yz}=\begin{pmatrix}1 & 0 & 0\\ 0 & 0 & 1\\ 0 & 1 & 0\end{pmatrix}\quad M_{xz}=\begin{pmatrix}0 & 0 & 1\\ 1 & 0 & 0\\ 0 & 1 & 0\end{pmatrix}$$

First, the three rotational symmetries C_{2z}、$C_{2x,}$ and C_{2y} lead that the linear optical conductivity tensor is

$$\sigma_{ij}=\begin{pmatrix}\sigma_{xx} & 0 & 0\\ 0 & \sigma_{yy} & 0\\ 0 & 0 & \sigma_{zz}\end{pmatrix}$$

Then, the three mirror symmetries M_{xy}、$M_{yz,}$ and M_{xz} lead to the linear optical conductivity tensor $\sigma_{xx}=\sigma_{yy}=\sigma_{zz}$.

Indeed, only three linear optical conductivity components in the zincblende structure are non-zero, and they are all equal.

Zincblende structure: Shift current tensor

$$\sigma_{ijk} = \begin{pmatrix} \sigma_{xxx} & \sigma_{xxy} & \sigma_{xxz} & \sigma_{xyy} & \sigma_{xyz} & \sigma_{xzz} \\ \sigma_{yxx} & \sigma_{yxy} & \sigma_{yxz} & \sigma_{yyy} & \sigma_{yyz} & \sigma_{yzz} \\ \sigma_{zxx} & \sigma_{zxy} & \sigma_{zxz} & \sigma_{zyy} & \sigma_{zyz} & \sigma_{zzz} \end{pmatrix}$$

When considering the three rotational symmetries, only the tensor containing *xyz* at the same time remains non-zero, resulting in the shift current tensor being reduced from the initial 18 components to just 3 tensors: σ_{xyz}, σ_{yxz}, and σ_{zxy}.

We need to examine the influence of the three mirror symmetries on these three remaining tensors.

Consider the M_{xy} mirror symmetry

$$M_{xy} = \begin{pmatrix} 0 & 1 & 0 \\ 1 & 0 & 0 \\ 0 & 0 & 1 \end{pmatrix}$$

$$\sigma_{xyz} = R_{xy}R_{yx}R_{zz}\sigma_{xxx} = (1)(1)(1)\sigma_{yxz} = \sigma_{yxz}$$

$$\sigma_{yzx} = R_{yx}R_{zz}R_{xy}\sigma_{xzy} = (1)(1)(1)\sigma_{xzy} = \sigma_{xzy}$$

$$\sigma_{zxy} = R_{zz}R_{xy}R_{yx}\sigma_{zyx} = (1)(1)(1)\sigma_{zyx} = \sigma_{zyx}$$

Then, consider the M_{yz} mirror symmetry

$$M_{yz} = \begin{pmatrix} 1 & 0 & 0 \\ 0 & 0 & 1 \\ 0 & 1 & 0 \end{pmatrix}$$

$$\sigma_{xyz} = R_{xx}R_{yz}R_{zy}\sigma_{xzy} = (1)(1)(1)\sigma_{xzy} = \sigma_{xzy}$$

$$\sigma_{yxz} = R_{yz}R_{xx}R_{zy}\sigma_{zxy} = (1)(1)(1)\sigma_{zxy} = \sigma_{zxy}$$

$$\sigma_{zxy} = R_{zy}R_{xx}R_{yz}\sigma_{yxz} = (1)(1)(1)\sigma_{yxz} = \sigma_{yxz}$$

Finally, consider M_{xz} mirror symmetry

$$M_{xz} = \begin{pmatrix} 0 & 0 & 1 \\ 1 & 0 & 0 \\ 0 & 1 & 0 \end{pmatrix}$$

$$\sigma_{xyz} = R_{xz}R_{yx}R_{zy}\sigma_{zxy} = (1)(1)(1)\sigma_{zxy} = \sigma_{zxy}$$

$$\sigma_{yxz} = R_{yx}R_{xz}R_{zy}\sigma_{xzy} = (1)(1)(1)\sigma_{xzy} = \sigma_{xzy}$$

$$\sigma_{zxy} = R_{zy}R_{xz}R_{yx}\sigma_{yzx} = (1)(1)(1)\sigma_{yzx} = \sigma_{yzx}$$

Therefore, ultimately, all three quantities are equal.

$$\sigma_{xyz} = \sigma_{yzx} = \sigma_{zxy}$$

References:

1. L. A. Palomino-Rojas, M. López-Fuentes, G. H. Cocoletzi, G. Murrieta, R. de Coss and N. Takeuchi, *Solid State Sciences*, 2008, **10**, 1228-1235.
2. S.-H. Wei and S. B. Zhang, *Physical Review B*, 2000, **62**, 6944-6947.
3. A. Jenichen, C. Engler and B. Rauschenbach, *Surface Science*, 2013, **613**, 74-79.
4. V. N. Jafarova, *International Journal of Modern Physics B*, 2022, **36**, 2250156.
5. S. Ferahtia, S. Saib and N. Bouarissa, *International Journal of Modern Physics B*, 2016, **30**, 1650147.
6. S. Hull and D. A. Keen, *Physical Review B*, 1999, **59**, 750.
7. D. Nath and R. Das, *Journal of Alloys and Compounds*, 2021, **879**, 160456.
8. K. Senthilkumar, T. Kalaivani, S. Kanagesan, V. Balasubramanian and J. Balakrishnan, *Journal of Materials Science: Materials in Electronics*, 2013, **24**, 692-696.
9. S.-H. Wei and S. B. Zhang, *Physical review B*, 2000, **62**, 6944.
10. S. A. Pochareddy, A. P. Nicholson, A. Thiyagarajan, A. Shah and W. S. Sampath, *Journal of Electronic Materials*, 2021, **50**, 2216-2222.
11. D. Ren, B. Xiang, Y. Gao, C. Hu and H. Zhang, *AIP Advances*, 2017, **7**.
12. Y. Asadi and Z. Nourbakhsh, *Computational Condensed Matter*, 2019, **19**, e00372.
13. D. D. Fan, H. J. Liu, L. Cheng, J. H. Liang and P. H. Jiang, *Journal of Materials Chemistry A*, 2018, **6**, 12125-12131.
14. D. R. Lide, *CRC handbook of chemistry and physics*, CRC press, 2004.
15. Ø. Johansen, V. Risinggård, A. Sudbø, J. Linder and A. Brataas, *Physical Review Letters*, 2019, **122**, 217203.